PERFORMANCE EVALUATION OF SOLAR BLIND NLOS ULTRAVIOLET COMMUNICATION SYSTEMS

Zhengyuan Xu
Department of Electrical Engineering, University of California
Riverside, CA 92521 USA
dxu@ee.ucr.edu

Brian M. Sadler
Army Research Laboratory, Adelphi, MD 20783 USA
bsadler@arl.army.mil

ABSTRACT

Ultraviolet (UV) systems provide unique opportunities for communications and sensing. We present recent results in UV communications, including experiments and analysis. We describe our experimental ultraviolet communication test-bed based on light emitting diodes with divergent beams, a solar blind filter, and a wide field-of-view detector. Then we report on statistical models for noise and signal photon counts, non-line of sight (NLOS) short-range ultraviolet communication link losses, and performance of photon counting detectors, operating in the solar blind spectrum regime. The effects of transmitter and receiver elevation angles, separation distance, and path loss are included. We also demonstrate shot-noise limited bit-error-rate performance, showing good agreement with analytically predicted performance.

1. INTRODUCTION

With the unique scattering and absorption properties of ultraviolet (UV) waves propagating through an atmospheric channel, the UV spectrum provides unique opportunities for diverse short-range communication environments, including line-of-sight (LOS) and non-line-of-sight (NLOS) channels [1][2]. By operating in the solar blind region [3], a wide field-of-view (FOV) receiver can exploit the very low solar background to achieve excellent signal-to-noise ratio (SNR) and quantum noise limited photon-counting detection. These benefits can now begin to be realized based on technological advances in both miniaturized low-power solid-state UV devices and advanced UV communications technology. In this paper, we present experimental and analytical performance evaluation of a solar blind, non-LOS outdoor UV communications link.

Ultraviolet communications has a rich research history (e.g., see the recent survey in [4]). Relevant studies date back to the 1960's [5][6], and later included experimental characterization of a scattering-based UV link [7], analytical channel modeling [8], a NLOS UV voice communication system, and a local area network demonstration [9][10][11]. All these UV systems used a flashtube/lamp/laser as a light source; these devices are bulky, power hungry, or bandwidth limited. Semiconductor UV optical sources offer potential low cost, small size, low power, high reliability, and high bandwidth. Recent efforts such as the DARPA Semiconductor UV Optical Source (SUVOS) program have led to commercialized (research-grade) deep UV LEDs (e.g., Sensor Electronics Technology Co.) [12]. A typical UV LED radiates an average optical power of 1 mW.

To develop an effective outdoor communication transceiver under exposure to solar radiation, solar-blind UV detection and filtering technology is crucial to maximally suppress out-of-band radiation. Commercial UV photomultiplier tubes (PMTs) achieve a very high multiplication gain of 10^5~10^7, high responsivity of 62 A/W, large detection area of a few cm^2, reasonable quantum efficiency of 15%, and low dark current of 0.1 nA/cm^2 (only about 10^2 dark counts per second). These features enable detection of very weak signals, even with the detector pointing directly at the sun, down to single photon counting resolution. An off-the-shelf solar blind filter, combined with a solar blind PMT, typically yields an excellent out-of-band rejection ratio of about 10^8. Solid state avalanche photodiode (APD) detectors are also rapidly being developed, e.g., through the DARPA Deep Ultraviolet Avalanche Photodetector (DUVAP) program, that aims to demonstrate APD arrays with performance metrics comparable to a typical PMT.

The availability of deep UV LEDs, solar blind PMTs and filters has inspired recent research on LED based UV system performance for applications from short range communications to sensing and imaging. Potential military applications include unattended ground sensor (UGS) networks and small unit communications, flame sensing, biological fluorescence detection, missile or artillery/gun fire detection, ground-air communications, optical tag identification, and covert networking [4]. In a mobile ad-hoc network, UV's enhanced geographic coverage with a reasonable transmitter beam divergence and wide receiver FOV could enable terminals on–the-move to more readily

Report Documentation Page

Form Approved
OMB No. 0704-0188

1. REPORT DATE	2. REPORT TYPE	3. DATES COVERED
01 DEC 2008	**N/A**	**-**

4. TITLE AND SUBTITLE	5a. CONTRACT NUMBER
Performance Evaluation Of Solar Blind NLOS Ultraviolet Communication Systems	5b. GRANT NUMBER
	5c. PROGRAM ELEMENT NUMBER
6. AUTHOR(S)	5d. PROJECT NUMBER
	5e. TASK NUMBER
	5f. WORK UNIT NUMBER
7. PERFORMING ORGANIZATION NAME(S) AND ADDRESS(ES) **Department of Electrical Engineering, University of California Riverside, CA 92521 USA**	8. PERFORMING ORGANIZATION REPORT NUMBER
9. SPONSORING/MONITORING AGENCY NAME(S) AND ADDRESS(ES)	10. SPONSOR/MONITOR'S ACRONYM(S)
	11. SPONSOR/MONITOR'S REPORT NUMBER(S)

12. DISTRIBUTION/AVAILABILITY STATEMENT
Approved for public release, distribution unlimited

13. SUPPLEMENTARY NOTES
See also ADM002187. Proceedings of the Army Science Conference (26th) Held in Orlando, Florida on 1-4 December 2008, The original document contains color images.

14. ABSTRACT

15. SUBJECT TERMS

16. SECURITY CLASSIFICATION OF:			17. LIMITATION OF ABSTRACT	18. NUMBER OF PAGES	19a. NAME OF RESPONSIBLE PERSON
a. REPORT	b. ABSTRACT	c. THIS PAGE			
unclassified	**unclassified**	**unclassified**	**UU**	**7**	

maintain connectivity, in contrast to a conventional optical system with a much stricter pointing and tracking requirement. Atmospheric attenuation, and eye safety limits, make such a link appropriate for ranges on the order of 1 km or less, and are inherently covert.

2. EXPERIMENTAL SETUP

The University of California, Riverside (UCR) has recently built a NLOS UV communications test-bed under support of the Army Research Office and in collaboration with the Army Research Laboratory [4][13][14], as pictured in Fig. 1. The transmitter uses a waveform generator feeding binary sequences to current driver circuitry that powers an array of 7 ball-lens UV LEDs. Each LED receives a driving current of 30 mA, yielding an average radiated optical power of 0.3 mW. The beam angular distribution was found to follow a superposition of multiple Gaussian functions with a full divergence angle of 10°. The LEDs (UVTOP250 with nominal center wavelengths of 250 nm) are mounted on a calibrated plate.

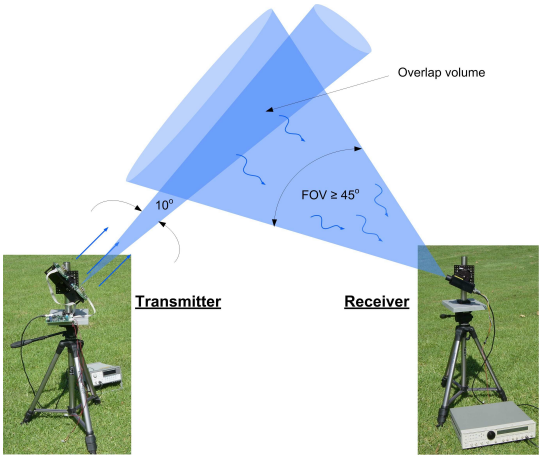

Fig. 1. UCR non-line-of-sight UV communications test-bed.

At the receiver, either a PMT or APD detector may be used. For the results reported here, we employed a solar-blind filter combined with a PMT for photon detection. The solar blind filter was placed in front of the sensing window of a PerkinElmer PMT module MP1922 (head-on window). The filter has a full-width half-maximum (FWHM) bandwidth of 15 nm with peak transmission of 10.4% at 255 nm. The spectral mismatch between the LED and the filter was found to be less than 30%. The PMT has a circular sensing window with a diameter of 1.5 cm, resulting in an active detection area of 1.77 cm^2, and it has an average of 10 dark counts per second (10 Hz). The composite in-band UV transmission of PMT plus filter was found to be 1%. The detector's effective FOV was estimated to be about 30°. The PMT output current was directed to a low noise amplifier followed by a photon counter unit. Note that some spectral mismatch loss between the LEDs and the filter was unavoidable due to practical device constraints. A mechanical module at Tx/Rx uses two perpendicular rotation stages to achieve high-resolution angular control in both azimuth and zenith directions.

3. EXPERIMENTAL RESULTS

We first characterize the solar background noise and signal count statistical distributions. Then we further link key system parameters such as path loss and communication bit error rate (BER) under different transmitter (Tx) and receiver (Rx) geometries.

3.1 Solar irradiance and signal count distributions

Solar noise and signal count distributions are important for power budget calculations and system design. In our outdoor experiments, the dark count rate of the PMT was negligible when compared with the count rates due to solar radiation in the deep UV band and the received signal. Measurements of the maximum solar radiation noise counts were recorded as the PMT was aimed directly towards the sun at noon. The time interval for measurements was set to be 200 μs (a rate of 5 kHz). This value was set to achieve reasonably high signal levels (i.e., the number of signal counts) per pulse for a variety of test geometries. Each observation window was segmented into several time intervals. The received solar noise counts within each time window were then recorded. Measurements from dozens of time windows were used to obtain the distribution of the random noise photon counts.

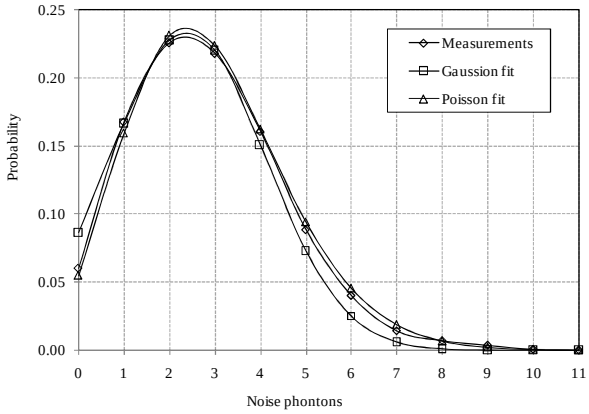

Fig. 2. Distribution of solar radiation photon counts.

In Fig. 2, experimental results are compared against a best-fit Poisson distribution and a best-fit truncated Gaussian distribution. The Gaussian distribution is found to have a mean of 2.9 counts and a standard deviation of 1.8 counts per interval. This yields an average noise count rate of 14.5 kHz with standard deviation equal to 9 kHz. The Poisson distribution has the same mean. It is found that both fitting errors are below 2%, but the Poisson fit is somewhat better. However, for simplicity of communication performance analysis, we adopt a Gaussian distribution as a

reasonable approximation. It is worth mentioning that the measured solar background count represents the total contribution of solar radiation over a range of wavelengths below 320 nm, and is not necessarily only due to in-band noise, because the PMT and filter still have out-of-band leakage. Consequently, the system detected non-negligible solar radiation.

The above measurement results indicate that, in order for our receiver to achieve an SNR of 10 dB or more, the received signal count rate should be greater than F=145 kHz, on average. This rate can be translated into an average received power for a given transmission wavelength. Each photon carries a total energy, $E=hc/\lambda$ where h is the Planck constant, c is the speed of light, and λ is transmission wavelength. For example, a photon with λ=250 nm carries a total energy $E=7.956*10^{-19}$ J. Hence, to achieve 10 dB SNR the average received power must be no less than $P_r=E*F=1.15*10^{-13}$ W$=1.15*10^{-10}$ mW. For a single LED transmitting an average power of P_t=0.3 mW, the total system loss is thus required to be within $2.6*10^{9}$, or equivalently 94 dB. This includes propagation loss, filter loss, and PMT loss. If we consider the system to have a constant loss budget, however, increasing the number of LEDs helps to increase the received signal power in order to reach a desired signal photon count.

Under daytime operating conditions, the noise count rate varied from late morning to early afternoon by at most a factor of two, down to a photon count rate of 8 kHz. The rate, however, varied significantly with time over the course of one day. During several experiments it dropped to below 1 kHz in the early morning or late afternoon. Knowledge of noise count is needed to determine acceptable signal levels and maintain desired SNR at the receiver, especially when using photon counting receivers. If the data rate is increased, both the noise count and the signal count per pulse decrease. More transmit power is also needed if the pulse duration is made shorter to keep a constant number of signal photons per pulse. Note also that, at night, dark counts become the dominant noise source.

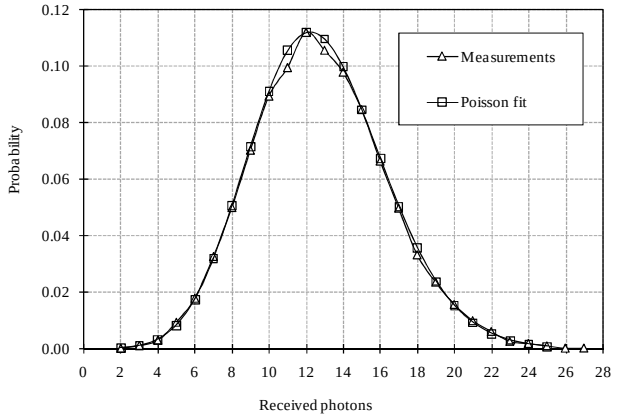

Fig. 3. Distribution of signal photon counts.

Signal counts were also recorded. The signal photon count measurements were obtained during the same times of day, with Tx/Rx elevation angles of 30°/30° and a separation distance of 70 m. Figure 3 shows both experimental data points and a Poisson curve fit for the signal photon counts. Very good agreement is apparent.

3.2 Path loss

Path loss measurements were obtained for different Tx/Rx geometries and separation distances. The path loss was calculated as the ratio between the transmitted photons radiated from the UV LEDs and the signal photons impinging upon the receiver. The former was calculated based on the measured source radiated power, and the latter was calculated from measured received photons divided by the total percentage loss from the filter and PMT. The receiving area was 1.77 cm^2. If path loss per unit area is of interest, then results can be normalized by this area.

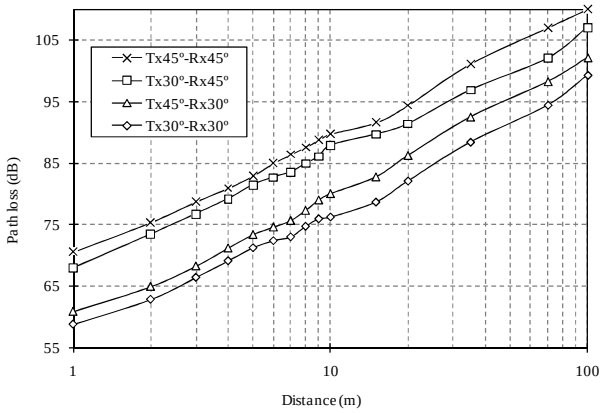

Fig. 4. Path loss versus distance, for different Tx and Rx elevation angles.

Figure 4 presents the path loss at different distances on a logarithmic scale, for different Tx and Rx elevation angles. We observe that the path loss increases by about 18 dB for each order of magnitude increase in distance r, i.e., path loss is proportional to $r^{1.8}$ under this geometry (the path loss exponent is 1.8). For other geometries, the path loss exponent may change. For example, for a very short range up to 10 m and Tx/Rx angle of 90°, it was found to be close to 1. However, the effect of geometry on the path loss exponent is still under investigation. For a fixed Rx angle, the loss is not very sensitive to the change in the Tx angle at these moderate angle values. A total variation of only a few decibels is observed when the Tx angle is changed from 30° to 45°. If we fix the Tx angle, however, the loss is found to depend highly on the Rx angle, with a 10 dB difference between Rx angles 30° and 45°. In general, as expected, we observe that the loss increases as either the Tx or Rx angle increases. This is due to the longer propagation path as well as the inherent scattering loss. In our experiments, the beam divergence and receiver FOV were fixed. They might also contribute to path loss variations, although their effects can

only be observed if additional optical modules to control those angles are designed and integrated with the LEDs and the filter.

It is worth mentioning that the separation distance (the LOS range between Tx and Rx) in our measurements is relatively short (up to 100 m). Because the attenuation coefficient is typically in the range of 1~10 km^{-1} [2], losses due to atmospheric attenuation were insignificant and thus not reflected in our measurements. However, if the separation distance is increased to multiple kilometers, atmospheric attenuation may become dominant, following the typical exponential power decay law assumed in the literature [2]. Such observations also suggest that attenuation effects can be neglected for short range communication systems (<1 km), and that scattering loss is dominant in this case.

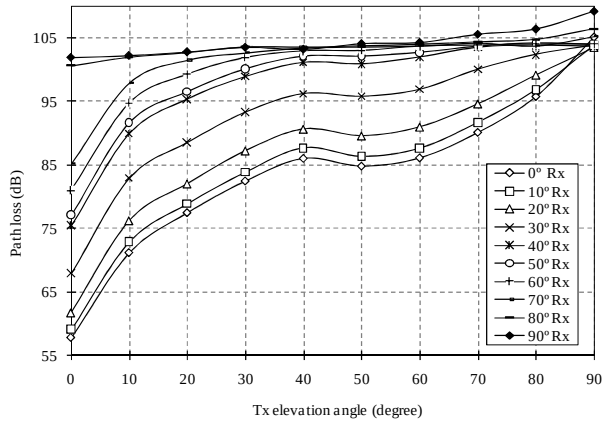

Fig. 5. Path loss versus Tx elevation angles for different Rx elevation angles.

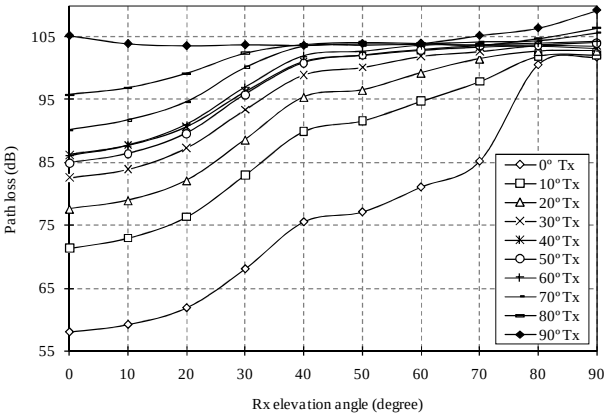

Fig. 6. Path loss versus Rx elevation angles for different Tx elevation angles.

We next investigate the path loss as a function of different Tx/Rx geometry. Measured results are shown in both Figs. 5 and 6, where the separation distance is fixed to 25 m, and we obtain the path loss as we vary the Tx and Rx elevation angles, respectively. Several observations can be made from each figure with regard to the properties of NLOS scattering communication systems. A total path-loss difference of over 50 dB is observed as the angle is changed from 0^o (LOS) to 90^o. The rate of change of the path loss decreases when the angle is increased and saturates at approximately 103 dB when the Tx/Rx angle is increased over 75°. Thus, path loss is more sensitive to angle variation when angles are small. The path loss is also observed to increase semi-monotonically with the variation of the Tx/Rx angle (x-axis) for a fixed Rx/Tx angle, with the exception of an observed minimum at around 50° Tx angle. This may be attributed to angular dependent scattering in the common volume, as represented by the scattering phase function [15]. The phase function which describes the angular distribution of the scattered beam is typically calculated as a weighted sum of both Rayleigh (molecular) and Mie (aerosol) scattering phase functions [15]. The weights can be chosen to be proportional to the corresponding scattering coefficients. Due to individual behaviors of Rayleigh and Mie scattering phase functions in the deep UV band, the averaged phase function shows a maximum at a certain scattering angle, indicating the strongest scattered UV radiation (or the smallest path loss) in that direction relative to the beam incident angle. This property suggests that the phase function may have a direct impact on the angular path loss behavior. While quantitative and qualitative analysis would be more convincing than the current reasoning, this approach is unavailable because it depends on a realistic phase function model and a path loss model. The path loss is also observed to be less sensitive to the dependent angle in the range of 30°~60° versus other values, partially explaining the angle insensitivity phenomenon in Fig. 4.

The path loss for special configurations of very large Tx/Rx elevation angles and very short distances can be approximated analytically from the single scattering impulse response model [8] and approximation for the intersected cone volume. It can then be compared with experimental results. Let us denote r as the Tx and Rx separation, θ_1 and θ_2 as the Tx and Rx elevation angles, ϕ_1 and ϕ_2 as the Tx beam angle and Rx FOV, k_e the extinction coefficient, k_s the scattering coefficient, $\theta_s=\theta_1+\theta_2$ as the angle between forward direction of incident waves and observation direction, A_r as the area of the receiving aperture, and $P(\mu)$ the scattering phase function where $\mu=\cos(\theta_s)$. For optical scattering, classical phase function models include an isotropic, Rayleigh (molecular) and Mie (aerosol) phase function given below [15]

$$p^{I}(\theta_s)=\frac{1}{4\pi},$$

$$p^{Ray}(\mu)=\frac{3[1+3\gamma+(1-\gamma)\mu^2]}{16\pi(1+2\gamma)},$$

$$p^{Mie}(\mu)=\frac{1-g^2}{4\pi}\left[\frac{1}{(1+g^2-2g\mu)^{3/2}}+f\frac{0.5(3\mu^2-1)}{(1+g^2-2g\mu)^{3/2}}\right]$$

where γ, g, and f are model parameters. Due to the existence of different types of particles in the atmosphere, neither of the above individual functions is suitable for a practical physical scattering process. Instead, the overall phase function to capture all particle effects can be modeled as a weighted sum of the Rayleigh and Mie scattering phase functions

$$P(\mu) = \frac{k_s^{Ray}}{k_s} p^{Ray}(\mu) + \frac{k_s^{Mie}}{k_s} p^{Mie}(\mu) \qquad (4)$$

according to the corresponding scattering coefficients k_s^{Ray} and k_s^{Mie} where $k_s = k_s^{Ray} + k_s^{Mie}$. Then after some mathematical manipulations, path loss is found to be

$$L \approx \frac{96 r \sin\theta_1 \sin^2\theta_2 \left(1 - \cos\frac{\phi_1}{2}\right) \exp\left[\frac{k_e r (\sin\theta_1 + \sin\theta_2)}{\sin\theta_s}\right]}{k_s P(\mu) A_r \phi_1^2 \phi_2 \sin\theta_s \left(12\sin^2\theta_2 + \phi_2^2 \sin^2\theta_1\right)}$$

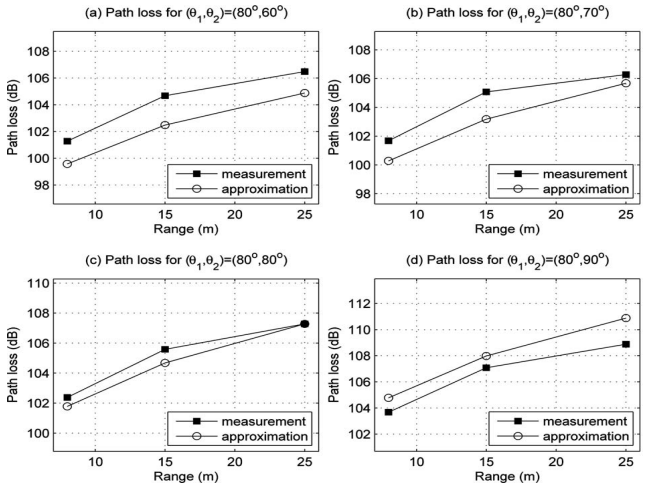

Fig. 7. Measured and predicted path losses per unit cm^2.

Path loss per unit area cm^2 versus short communication range is compared with measurement for different θ_2 in Fig. 7. The following geometric and model parameters were chosen: $(\phi_1,\phi_2,\theta_1)=(10^o,30^o,80^o)$, at wavelength λ=260 nm $(k_e, k_s^{Ray}, k_s^{Mie})=(1.39, 0.24, 0.25)$ km^{-1}, γ=0.017, g=0.72 and f=0.5. The larger θ_2, the closer the predicted path loss approaches measurement, with error from 2 dB down to 0dB. This indicates that the single scattering model well predicts link performance for short range and large apex angles. Experiments for longer range and larger apex angle are limited by the available LED emission power.

3.3 BER performance

Experiments were also conducted to measure the communication BER using on-off keying (OOK) modulation. The received signal model is described by $y=x+n$ where x is signal and n is noise. Demodulation was performed off-line after the received counts were recorded. The threshold used to decide whether a pulse was received or not was optimized based on the background noise and signal photon counts. Note that the SNR of the received signal is affected by the different geometric parameters described earlier. Therefore, to present the BER for different SNRs, we chose to vary the Tx and Rx angles in order to vary the SNR as desired. Considering the randomness of received signal and noise photons, the BER and SNR presented below are measured averages.

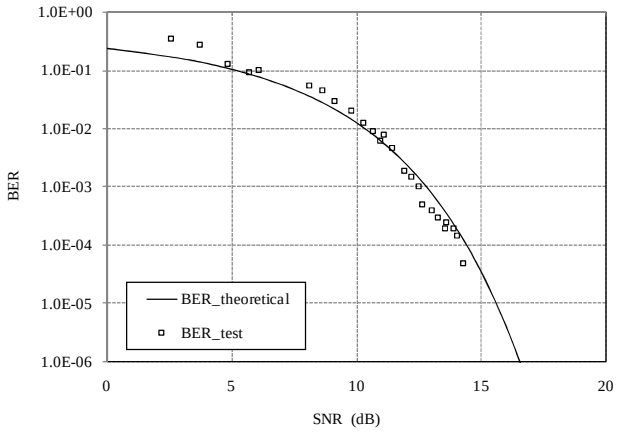

Fig. 8. BER for varying SNR.

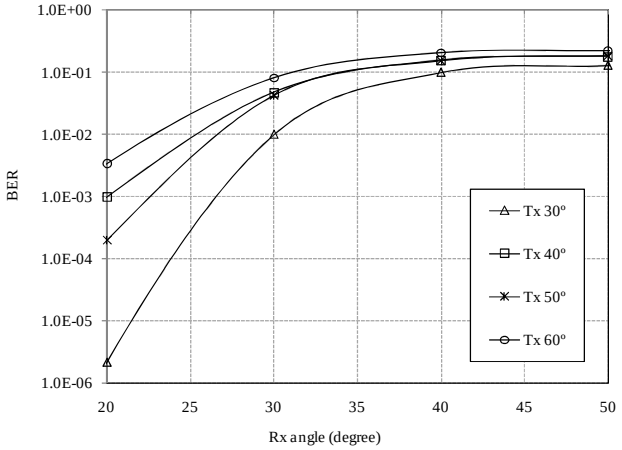

Fig. 9. BER versus Rx elevation angles for different Tx elevation angles.

Figure 8 compares measured and predicted BER, where the prediction is based on the SNR and the Gaussian Q-function formula valid for Gaussian noise, which approximates the measured noise count distribution. Predicted and measured results show good agreement. This figure also reveals how much received SNR is required to achieve a certain BER, or equivalently the average required received signal photon count for a given noise environment. For example, at SNR=10 dB, a BER of 10^{-2} is achievable; and as SNR increases to 15 dB, a BER below 10^{-4} is achievable. To see how Rx elevation angle explicitly impacts BER, we fixed the Tx elevation angle at 30°, 40°, 50°, and 60°, respectively, at a communication distance of 35 m. Corresponding BER results are plotted in Fig. 9. The

figure illustrates that the BER with Tx angle fixed at 30° can drop from 10^{-1} to about 10^{-6} when the Rx angle decreases from 40° to 20°, with further reductions in BER when pointing approaches line-of-sight.

It is also possible to predict BER performance from the approximate path loss expression we developed earlier. Each photon carries energy hc/λ where c is the speed of light, and h is Planck's constant. The average detected number of signal photons per bit is $P_r\eta_f\eta_r\lambda/(Rhc)$ where η_f is the filter transmission, η_r the detector quantum efficiency, R the data rate, and P_r the received power obtained from transmitted power P_t as $P_r=P_t/L$. For direct detection by an ideal receiver, the BER under optimum detection of on-off keying signals is given

$$BER = 0.5\exp\left\{-\frac{P_t\eta_f\eta_r}{L(hc/\lambda)\,R}\right\}$$

as a function of the system parameters.

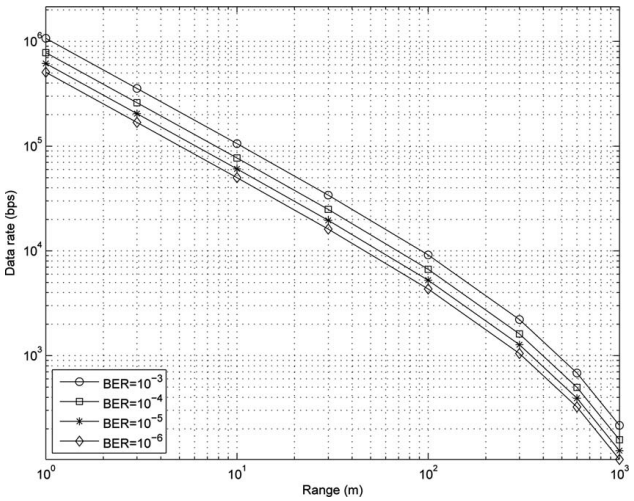

Fig. 10. Rate-range-BER tradeoffs.

We assume an LED array with power 50 mW, η_f =0.1, A_r=1.77 cm^2, η_r=0.2, $(\theta_1,\theta_2)=(30^o,30^o)$. The other parameters match Fig. 7. Figure 10 depicts data rate versus range, with curves parameterized by BER. For a raw BER (no coding) requirement of 10^{-3}, the corresponding data rate is 100 kbps at 10m range, and drops to 10 kbps at 100 m range. If path loss L is doubled (a 3dB increase) or transmitted power decreases by half, then the BER increases to $0.5(2\times10^{-3})^{0.5}=2.24\times10^{-2}$. Similarly, the impact of other system parameters on performance can be readily determined.

It is worth mentioning that the above results are based on the (30°,30°) Tx/Rx elevation angles in a NLOS setup. If the configuration changes to LOS, i.e., (0°,0°) elevation angles, then the SNR will increase by at least 35dB. Accordingly, either range or data rate will increase by 2~3 orders of magnitude (shift curves right or up by that order).

4. CONCLUSIONS

This paper presented various experimental and analytical results for NLOS UV communications based on low power divergent LED source arrays. Solar background noise and signal count distributions were characterized. The path loss and BER of corresponding photon counting detectors were studied under different system geometries determined by Tx and Rx elevation angles and communication distances. These experimental results are valuable for the design of practical receivers for NLOS systems.

Additional studies have been conducted [16] showing that path loss predictions based on the single scattering model [8] are only applicable to very limited geometries and significantly deviate from measurements under many other geometries. An appropriate multiple scattering model may prove to be more generally applicable. The path loss exponent may depend on geometry, beam profile, and Rx FOV. It may vary from a value close to 1 as reported in the literature [2][8][15], to a value close to 2 reported in the current work. Our continuing studies will focus on developing a path loss model [16], scattering and phase function models based on measurements under different meteorological conditions, incorporating the effects of beam angle and FOV. We are also studying the channel impulse response and atmospheric attenuation effects using a high power UV source.

ACKNOWLEDGEMENT

The authors would like to thank Gang Chen, Feras Abou-Galala, Haipeng Ding and Qunfeng He for their invaluable help. This work was supported in part by the Army Research Office under Grants W911NF-06-1-0364 and W911NF-06-1-0173, and the Army Research Laboratory under the Collaborative Technology Alliance Program, Cooperative Agreement DAAD19-01-2-0011.

REFERENCES

[1]. D. M. Reilly, D. T. Moriarty, and J. A. Maynard, "Unique properties of solar blind ultraviolet communication systems for unattended ground sensor networks," *Proc. of SPIE*, vol. 5611, pp. 244-254, October 2004.

[2]. G. A. Shaw, A. M. Siegel, and J. Model, "Extending the range and performance of non-line-of-sight ultraviolet communication links," *Proc. of SPIE*, vol. 6231, pp. 62310C.1-62310C.12, 2006.

[3]. L. R. Koller, *Ultraviolet Radiation*, 2nd ed., John Wiley & Sons, New York, 1965.

[4]. Z. Xu and B. M. Sadler, "Ultraviolet communications: potential and state-of-the-art," *IEEE Commun. Mag*. **46** (5), pp. 67-73, May 2008.

[5]. G. L. Harvey, "A survey of ultraviolet communication systems," Naval Research Laboratory Technical Report, Washington D.C., March 13, 1964.

[6]. J. A. Sanderson, "Optics at the Naval Research Laboratory," *Appl. Opt*. **6**, 2029-2043 (1967).

[7]. D. E. Sunstein, “A scatter communications link at ultraviolet frequencies,” B.S. Thesis, MIT, MA, 1968.

[8]. D. M. Reilly, “Atmospheric optical communications in the middle ultraviolet,” M.S. Thesis, MIT, MA, 1976.

[9]. E. S. Fishburne, M. E. Neer, and G. Sandri, “Voice communication via scattered ultraviolet radiation,” final report of Aeronautical Research Associates of Princeton, Inc., NJ, February 1976.

[10]. J. J. Puschell and R. Bayse, “High data rate ultraviolet communication systems for the tactical battlefield,” in *Proceedings of Tactical Communications Conf.* (April 1990), pp. 253-267.

[11]. B. Charles, B. Hughes, A. Erickson, J. Wilkins, and E. Teppo, “An ultraviolet laser based communication system for short range tactical applications,” *Proc. SPIE* **2115**, 79-86 (1994).

[12]. M. Shatalov, et al., “Deep ultraviolet light-emitting diodes using quaternary AlInGaN multiple quantum wells,” *IEEE J. Sel. Top. Quantum Electron.* **8**, 302-309 (2002).

[13]. Z. Xu, G. Chen, F. Abou-Galala, and M. Leonardi, “Experimental performance evaluation of non-line-of-sight ultraviolet communication systems,” *Proc. SPIE* 67090Y, 1-12 (2007).

[14]. G. Chen, F. Abou-Galala, Z. Xu, and B. M. Sadler, “Experimental evaluation of LED-based solar blind NLOS communication links,” *Optics Express*, September 2008.

[15]. Z. Xu, H. Ding, B. M. Sadler, and G. Chen, “Analytical performance study of solar blind non-line-of-sight ultraviolet short-range communication links,” *Optics Letters*, vol. 33, no. 16, pp.1860-1862, August 2008.

[16]. G. Chen, Z. Xu, H. Ding, and B. M. Sadler, “Path loss modeling and performance trade-off study for short-range non-line-of-sight ultraviolet communications,” *Optics Express*, August 2008 (submitted).